ISBN: 978-3-95450-208-0 doi:10.18429/JACoW-IPAC2019-FRXXPLS3

APPLICATION OF A PHASE SPACE BEAM POSITION AND SIZE MONITOR FORSYNCHROTRON RADIATION

N. Samadi†[1], University of Saskatchewan, Saskatoon, Canada
X. Shi, Advanced Photon Source, Argonne National Laboratory, Lemont, USA
L. Dallin, Canadian Light Source, Saskatoon, Canada
D. Chapman[1], University of Saskatchewan, Saskatoon, Canada
[1]also at Canadian Light Source, Saskatoon, Canada

Abstract

We report on a system (ps-BPM) that can measure the electron source vertical position and angular motion along with the vertical source size and angular size at a single location in a synchrotron bend magnet beamline. This system uses a combination of a monochromator and a filter with a K-edge to which the monochromator was tuned in energy. Measurement of the vertical beam location without the absorber and vertical edge location with the absorber allows measurement of the source position and angle. The beam width and edge width give information about the vertical electron source size and angular distribution. In this work, we show a typical measurement with the ps-BPM monitor and results that can be obtained from a single measurement. By combining the analysis in the time and frequency domain, information on beam motion and size can be extracted and identified. Examples of ps-BPM applications are given.

INTRODUCTION

Accurate measurements of the electron source size and divergence are becoming increasingly important at synchrotron facilities as the new generation light sources are being built with the focus on achieving the smallest possible emittance [1, 2].

Currently available ways of measuring the source size are relying on direct imaging or interference-based techniques. Direct imaging includes pinhole imaging [3, 4], imaging with Kirkpatrick-Baez (KB) mirrors [5], Compound Refractive Lenses (CRLs) [6] and Fresnel Zone Plates (FZP) [7, 8]. The interferometry based systems include double-slit diffraction [9-11], grating interferometry [12, 13], and π-polarization [14].

In addition to the importance of measuring the source size at these new generation light sources, beam stability is also of great concern. Real-time measurements of the position and angular position of the electron beam at a single location will be a powerful tool as a monitor, a diagnostic element and in a feedback system.

Here we present a new system, phase space Beam Position Monitor (ps-BPM), that measures, in real time, all four quantities (size, divergence, position, and angular position) of the electron source in the vertical plane from a single measurement [15, 16].

† Nazanin.samadi@usask.ca

ps-BPM SYSTEM

The ps-BPM system uses the nearly monochromatic beam provided by a crystal monochromator (in Bragg or Laue geometry) around an absorption K-edge of a selected filter element. Half of the horizontal fan of the beam is covered by the K-edge filter and the other half has no filter. Both halves of the beam are imaged with an area detector.

The unfiltered beam side of the image is summed over a horizontal width and the beam profile is shown in Fig. 1a. This profile is fitted with a Gaussian function from which the center location and the width of the beam are obtained.

For the filtered beam side the image data is also summed over a horizontal width as shown in Fig. 1b. This profile is then normalized by the unfiltered beam. The negative logarithm of this normalized filtered beam profile is taken to convert the filtered data to an absorption profile which resembles the step function associated with the K-edge of the element as shown in Fig. 1c. A spatial derivative is taken of this step-like function forming a peak which is then also fit by a Gaussian function from which we have an edge location and width as shown in Fig. 1d.

SOURCE POSITION AND ANGLE MEASUREMENTS

Filtered K-edge Side

It's been shown previously [15] that the location of the K-edge on the filtered K-edge side of the data is only sensitive to the electron beam position and not to the angular position of the electron beam. Therefore, the center of the Gaussian fit of the filtered K-edge side (y_{edge}) is a measure of the electron beam position (y_e) as shown in Eq. 1,

$$y_e = y_{edge} \,. \tag{1}$$

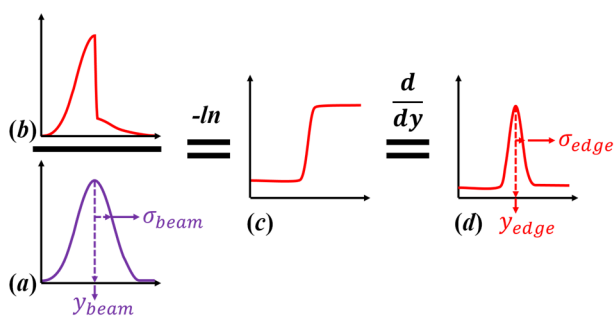

Figure 1: Beam and edge analysis of the ps-BPM system.

Content from this work may be used under the terms of the CC BY 3.0 licence (© 2019). Any distribution of this work must maintain attribution to the author(s), title of the work, publisher, and DOI

ISBN: 978-3-95450-208-0 doi:10.18429/JACoW-IPAC2019-FRXXPLS3

Unfiltered Side

The unfiltered beam side of the data includes the position and angular position of the electron source by,

$$y_{beam} = Dy'_e + y_e \,, \quad (2)$$

where D is the source-to-detector distance.
By having the two measurements at the same time, the angular position of the source (y'_e) can be solved as,

$$y'_e = (y_{beam} - y_{edge})/D \,. \quad (3)$$

SOURCE SIZE AND DIVERGENCE MEASUREMENTS

Filtered K-edge Side

The spatial width of the Gaussian fit from the filtered K-edge side of the beam, σ_{edge}, includes contributions from the natural width of the K-edge filter element, $\sigma_{y'_{K-edge}}$, the angular acceptance of the monochromator, $\sigma_{y'_{mono}}$ and the vertical size of the electron source, σ_y, all added in quadrature as,

$$\sigma^2_{edge} = \sigma^2_y + (D\sigma_{y'_{K-edge}})^2 + (D\sigma_{y'_{mono}})^2 \,. \quad (4)$$

The electron source size is then (Eq. 5),

$$\sigma_y = \sqrt{\sigma^2_{edge} - \left(D\sigma_{y'_{K-edge}}\right)^2 - \left(D\sigma_{y'_{mono}}\right)^2} \,. \quad (5)$$

Unfiltered Side

The measured spatial width of the unfiltered side, σ_{beam}, is the combination of the electron source size, σ_y, divergence, $\sigma_{y'}$, and the opening angle of the photon beam, $\sigma_{y'_{Ph}}$, added in quadrature as,

$$\sigma^2_{beam} = \sigma^2_y + (D\sigma_{y'})^2 + (D\sigma_{y'_{Ph}})^2 \,. \quad (6)$$

By having the opening angle of the photon beam, modelled as a Gaussian, and the measured σ_y from the edge side, we can solve for the divergence of the electron source,

$$\sigma_{y'} = \frac{1}{D}\sqrt{\sigma^2_{beam} - \sigma^2_y - (D\sigma_{y'_{Ph}})^2} \,. \quad (7)$$

This shows by having measurements of the unfiltered beam side and the filtered K-edge side we can measure the vertical position, angle, size and divergence of the electron source at the same time. However, to arrive at these values the contributions from $\sigma_{y'_{K-edge}}$, $\sigma_{y'_{mono}}$ and $\sigma_{y'_{Ph}}$ need to be determined and is presented elsewhere [16].

RESULTS

Two examples of the application of the ps-BPM system are presented to illustrate the ability to provide information regarding the source and even beamline properties.

Normal Operations

A typical measurement using the ps-BPM monitoring system is shown here to demonstrate the full characterization of the electron beam in the vertical direction during normal operations of the CLS facility. The measurement was performed at the Biomedical Imaging and Therapy (BMIT) bend magnet (BM) beamline [17-19] at the Canadian Light Source. The photon energy is tuned to the barium K-edge at 37.441 keV by the Si (220) Double Crystal Monochromator (DCM). The barium filter projected concentration is 35 mg·cm^{-2}. The images of the filtered and unfiltered beam were recorded by a flat panel Hamamatsu detector (Hamamatsu Photonics, Hamamatsu City, Shizuoka Pref., Japan) at D = 20 m from the source. The detector pixel size is 100×100 μm. A total of 3000 images were taken with an acquisition time of 0.03 s for each image.

The measurement results are shown in Fig. 2. The source position (y_e) and angular position projected at the detector location (Dy'_e) are shown as a function of time in Fig. 2a. The numbers shown on the figures are the standard deviation of the two positions over the entire measurement period of 90 s. The standard deviation values are the direct evaluation of the amplitude of beam motion. At the detector location, the angular motion of the source has larger effect than the source position motion.

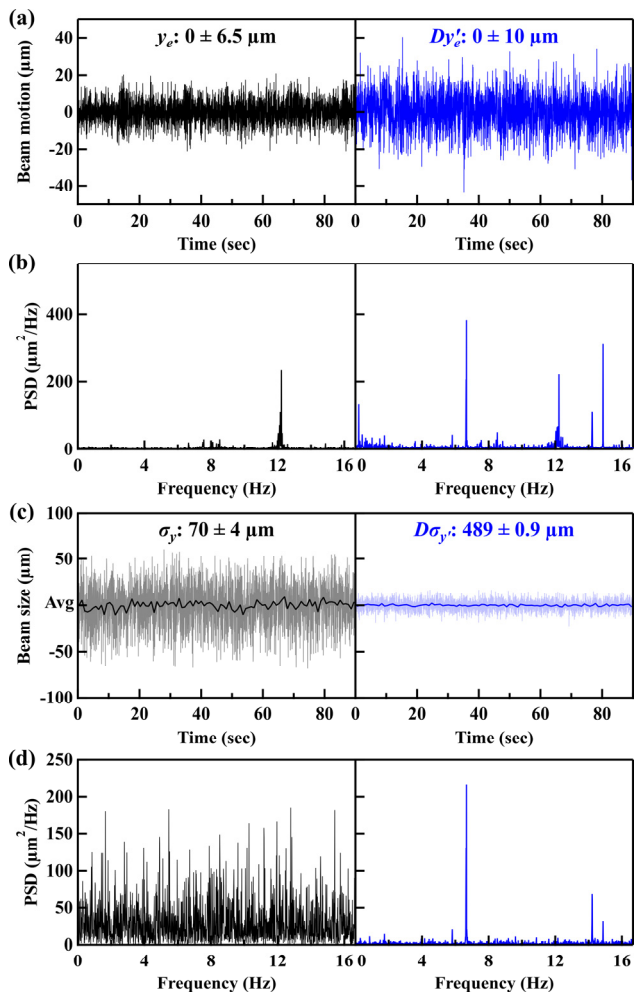

Figure 2: (a) The time evolution of y_e (left) and Dy'_e (right). (b) PSD functions of the two curves in (a). (c) The time evolution of σ_y (left) and $D\sigma_{y'}$ (right). The light colored and dark colored curves are for sampling time of 0.03 s and 0.9 s, respectively. (d) PSD functions of the light colored curves in (c).

Content from this work may be used under the terms of the CC BY 3.0 licence (© 2019). Any distribution of this work must maintain attribution to the author(s), title of the work, publisher, and DOI

ISBN: 978-3-95450-208-0 doi:10.18429/JACoW-IPAC2019-FRXXPLS3

Content from this work may be used under the terms of the CC BY 3.0 licence (© 2019). Any distribution of this work must maintain attribution to the author(s), title of the work, publisher, and DOI

The power spectral distribution (PSD) function, obtained from the Fourier transform of the time-dependent signal, allows characterizing the measured beam position in the frequency domain. The PSD functions of the two curves in Fig. 2a are shown in Fig. 2b, respectively. With the sampling rate of 33 Hz, positional variations or vibrations up to 16.7 Hz can be detected. The beam position shows three characteristic peaks at 6.7, 14.2 and 14.9 Hz, which are clearly from the angular motion. The small frequency band around the 12.2 Hz peak shows up in both the source position and angular position.

The source size (σ_y) and angular distribution projected on the detector ($D\sigma_{y'}$) are shown as a function of time in Fig. 2c. All curves are offset to their own average values, which are indicated in the figure. The light colored curves are plotted in the original time scale (0.03 s steps). Since the beam size measurements are photon hungry, a longer acquisition time is needed to improve its sensitivity [16]. In Fig. 2c, the over plotted curves with dark colors were obtained by averaging every 30 points (0.9 s). The standard deviation values shown in the figure are also for the averaged curves which show the sensitivity of the system for each of the three parameters. An integration of 0.9 s is adequate to reach the sensitivity of 4 μm for source size measurement.

The corresponding PSD functions of the fast measurement data (light colored curves in Fig. 2c) are shown in Fig. 2d. The PSD function for σ_y shows only random noise indicating that the present system is not fast enough to monitor source size changes on the millisecond scale. On the other hand, the PSD function for $D\sigma_{y'}$ shows clear frequency peaks that are consistent with the ones observed in the position plots (see Fig. 2b) which is an indication of adequate sensitivity.

BMIT Wiggler Field Changes

The next example looks at the effects of the BMIT wiggler on the BM source as the field is changed. The experiment was performed at the Iodine K-edge (33.169 keV) by the Si (220) DCM at the beamline. The iodine filter projected concentration is 60 mg·cm^{-2}. The BM source parameters were measured at different magnetic fields of the BMIT wiggler.

The extracted source size, divergence, position, and angular position are shown in Fig. 3 as a function of the wiggler field. All results are an average of 24 s. Varying the magnetic field of the wiggler alters the tune of the electron beam lattice which changes the source parameters at the BM location. Figure 3a and 3b show the motion of the electron beam position and angle, respectively. Fig. 3c shows a continuous reduction in the BM source size as the wiggler field increases. On the other hand, the source divergence decreases at the beginning and reaches its minimum after the wiggler field raises above 2 T as shown in Fig. 3d.

CONCLUSION

We have shown how to use the ps-BPM system to characterize source properties. The capability of monitoring source position, angular position, size, and divergence simultaneously is the unique feature of the ps-BPM monitor. Combining the time and frequency domain studies, the ps-BPM monitor can provide more systematic information about the source and the beamline.

The system was used during (1) normal operations where beam motions were found that are currently being looked at to identify their origins and (2) while an insertion device field was changed to assess the impact on beam motion and source size.

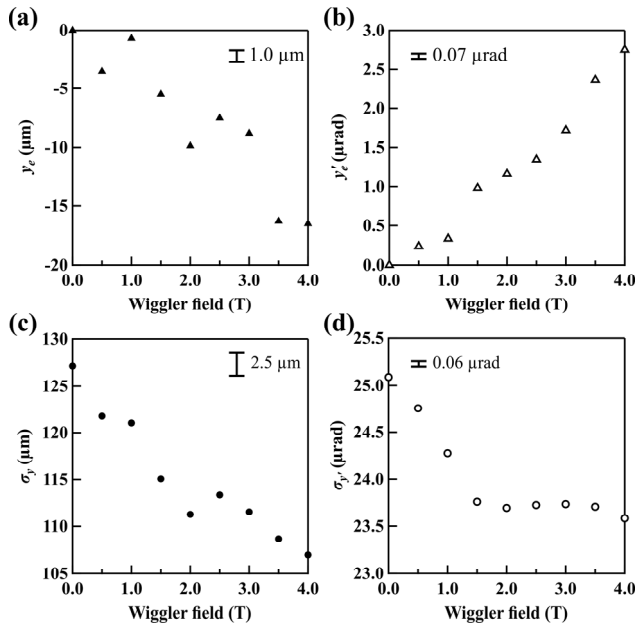

Figure 3: Extracted (a) σ_y, (b) $\sigma_{y'}$, (c) y_e, and (d) y_e' as a function of the magnetic field of the BMIT wiggler. The error bars are the standard deviation of 8 measurements of 3 s data.

ACKNOWLEDGEMENTS

The authors acknowledge the financial support of Canada Research Chair Program. The research described in this paper was performed at the Canadian Light Source, which is funded by the Canada Foundation for Innovation, NSERC, the National Research Council Canada, CIHR, the Government of Saskatchewan, Western Economic Diversification Canada, and the University of Saskatchewan. This work was also supported by the U.S. Department of Energy, Office of Basic Energy Sciences, under Contract No. DE-AC02-06CH11357.

REFERENCES

[1] P. F. Tavares, S. C. Leemann, M. Sjostrom, and A. Andersson, "The MAX IV storage ring project", *Journal of Synchrotron Radiation,* vol. 21, pp. 862-877, 2014.

[2] M. Eriksson, J. F. van der Veen, and C. Quitmann, "Diffraction-limited storage rings - a window to the science of tomorrow", *Journal of Synchrotron Radiation,* vol. 21, pp. 837-842, 2014.

[3] P. Elleaume, C. Fortgang, C. Penel, and E. Tarazona, "Measuring Beam Sizes and Ultra-Small Electron

ISBN: 978-3-95450-208-0 doi:10.18429/JACoW-IPAC2019-FRXXPLS3

Emittances Using an X-ray Pinhole Camera", *Journal of synchrotron radiation,* vol. 2, pp. 209-214, 1995.

[4] C. Thomas, G. Rehm, I. Martin, and R. Bartolini, "X-ray pinhole camera resolution and emittance measurement", *Physical Review Special Topics-Accelerators and Beams,* vol. 13, p. 022805, 2010.

[5] T. Renner, H. Padmore, and R. Keller, "Design and performance of the ALS diagnostic beamline", *Review of Scientific Instruments,* vol. 67, pp. 3368-3368, 1996.

[6] T. Weitkamp, O. Chubar, M. Drakopoulos, I. Snigireva, A. Snigirev, C. Schroer, *et al.*, "Electron Beam Size and Profile Measurements With Refractive X-Ray Lenses", in *Proceedings of EPAC*, 2000, pp. 1824-1826.

[7] K. Iida, N. Nakamura, H. Sakai, K. Shinoe, H. Takaki, M. Fujisawa, *et al.*, "Measurement of an electron-beam size with a beam profile monitor using Fresnel zone plates", *Nuclear Instruments and Methods in Physics Research Section A: Accelerators, Spectrometers, Detectors and Associated Equipment,* vol. 506, pp. 41-49, 2003.

[8] S. Takano, M. Masaki, and H. Ohkuma, "X-ray imaging of a small electron beam in a low-emittance synchrotron light source", *Nuclear Instruments and Methods in Physics Research Section A: Accelerators, Spectrometers, Detectors and Associated Equipment,* vol. 556, pp. 357-370, 2006.

[9] T. Mitsuhashi, *Beam Measurement: Proceedings of the Joint US-CERN-Japan-Russia School on Particle Accelerators, Montreux, and CERN, Switzerland*: World Scientific Publishing Company, 1999.

[10] T. Naito and T. Mitsuhashi, "Very small beam-size measurement by a reflective synchrotron radiation interferometer", *Physical Review Special Topics-Accelerators and Beams,* vol. 9, p. 122802, 2006.

[11] W. J. Corbett *et al.*, "Transverse Beam Profiling and Vertical Emittance Control with a Double-Slit Stellar Interferometer", in *Proc. 5th Int. Beam Instrumentation Conf. (IBIC'16)*, Barcelona, Spain, Sep. 2016, pp. 236-239. doi:10.18429/JACoW-IBIC2016-MOPG70

[12] J. P. Guigay, S. Zabler, P. Cloetens, C. David, R. Mokso, and M. Schlenker, "The partial Talbot effect and its use in measuring the coherence of synchrotron X-rays", *Journal of synchrotron radiation,* vol. 11, pp. 476-482, 2004.

[13] X. Shi, S. Marathe, M. J. Wojcik, N. G. Kujala, A. T. Macrander, and L. Assoufid, "Circular grating interferometer for mapping transverse coherence area of X-ray beams", *Applied Physics Letters,* vol. 105, p. 041116, 2014.

[14] Å. Andersson, M. Böge, A. Lüdeke, V. Schlott, and A. Streun, "Determination of a small vertical electron beam profile and emittance at the Swiss Light Source", *Nuclear Instruments and Methods in Physics Research Section A: Accelerators, Spectrometers, Detectors and Associated Equipment,* vol. 591, pp. 437-446, 2008.

[15] N. Samadi, B. Bassey, M. Martinson, G. Belev, L. Dallin, M. de Jong, *et al.*, "A phase-space beam position monitor for synchrotron radiation", *J Synchrotron Radiat,* vol. 22, pp. 946-55, Jul 2015.

[16] N. Samadi, X. Shi, L. Dallin, and D. Chapman, "A Real Time Phase-Space Beam Emittance Monitoring System", *Journal of Synchrotron Radiation,* p. Accepted 2019.

[17] T. W. Wysokinski, D. Chapman, G. Adams, M. Renier, P. Suortti, and W. Thomlinson, "Beamlines of the Biomedical Imaging and Therapy Facility at the Canadian Light Source - Part 2", *Journal of Physics: Conference Series,* vol. 425 Part 7, 2013.

[18] T. W. Wysokinski, D. Chapman, G. Adams, M. Renier, P. Suortti, and W. Thomlinson, "Beamlines of the biomedical imaging and therapy facility at the Canadian light source—Part 1", *Nuclear Instruments and Methods in Physics Research Section A: Accelerators, Spectrometers, Detectors and Associated Equipment,* vol. 582, pp. 73-76, 2007.

[19] T. W. Wysokinski, D. Chapman, G. Adams, M. Renier, P. Suortti, and W. Thomlinson, "Beamlines of the biomedical imaging and therapy facility at the Canadian light source - part 3", *Nuclear Instruments & Methods in Physics Research Section a-Accelerators Spectrometers Detectors and Associated Equipment,* vol. 775, pp. 1-4, Mar 1 2015.

Content from this work may be used under the terms of the CC BY 3.0 licence (© 2019). Any distribution of this work must maintain attribution to the author(s), title of the work, publisher, and DOI